Probing plasmon excitations in copper nano-clusters with spectroscopic ellipsometry

Erwin Zoethout

DIFFER - Dutch Institute for Fundamental Energy Research, De Zaale 20, 5612 AJ Eindhoven, the Netherlands

Abstract

Light induced *plasmon excitations* of copper nano-clusters have been probed using spectroscopic ellipsometry. Copper clusters of typically 20 nm diameter were created on the surface of a silicon wafer by means of physical vapour deposition. The growth of the clusters as well as the chemical interaction with atmosphere are monitored. Clear *plasmon excitations* are observed with resonance positions in the range from 1.85 to 2.1 eV for copper in its metallic state. The resonance position and amplitude scale linear with deposited amounts. Changes in resonance position and amplitude are observed when copper nano-clusters are exposed to atmosphere and a sub-nanometer thin copper oxide is formed. The resonance position red-shifts 0.4 eV (180 nm wavelength) after one day of exposure with respect to its metallic state. Spectroscopic ellipsometry is shown to have good sensitivity to ultra-thin (down to sub-nanometer thick) metal-oxide layers as well as to nanometer size changes of the copper nano-clusters. This puts the technique in a position where real-time monitoring of plasmon active material in gaseous or liquid environments of, for example, (photo-) catalytic processes becomes accessible.

1. Introduction

Understanding the interaction of light and matter is a challenging task at best, especially when looking at wavelengths near the visible part of the solar spectrum. Inter- and intraband electron transitions together with non-linear effects (*plasmon excitations*) are happening within this wavelength range. It is however an interesting range not only for creating beautifully coloured antique artefacts [1], but also for the more recent applications in photovoltaics and photo-catalysis [2-6] or photo-sensors [7].

Spectroscopic ellipsometry can be a useful tool to probe the optical performance of a reflective medium. In this paper we will demonstrate how ellipsometry can be used to probe *plasmon excitations*. This will be demonstrated by using copper nano-clusters as an example. Recently, copper clusters attracted attention for both catalytic as well as plasmonic activity [8]. Especially interaction with visible light induces an extra catalytic activity based on plasmon de-excitations. Plasmon (de-) excitations within the copper cluster can transfer energy by generating hot electrons, causing inter- and intra-band transitions in adsorbed molecules, by formation of electron-hole pairs, or by electron-phonon scattering induced heating [3]. The wavelength range and the intensity where *plasmon excitations* are active, differs dramatically depending on the copper (nano) cluster size and its direct environment [8-10]. Furthermore, the chemical state of copper is important for the optical response. This has been topic of many recent studies [11-13] that show the optical properties, including plasmonic activity, to depend critically on the oxidation state of the copper. This is especially relevant when examining copper after exposure to reactive molecules of, for example, atmospheric conditions. Complicating interpretation of copper's optical properties even further is the plasmon activity of cuprite (Cu_2O) [14], one of the species that forms already at room temperature [11-13]. The copper nano-clusters in this paper have therefore been topic of extensive in-situ and ex-situ material characterization.

This paper describes how the optical properties (permittivity) of copper nano-clusters near the visible part of the solar spectrum can be extracted and interpreted. The small morphological changes introduced by different deposited amounts or variable growth rate of copper's Volmer-Weber growth will show the sensitivity of the used spectroscopic ellipsometer technique to *plasmon excitations* in metallic copper. By using atmospheric exposure (ex-situ) to chemically modify the surface of the copper nano-clusters, the sensitivity of spectroscopic ellipsometry to ultra-thin metal-oxide shells is demonstrated.

2. Experimental details

2.1. Vacuum setup and in-situ techniques

In order to assure the chemical state of the material under investigation, all samples were prepared in an ultra-high vacuum (UHV) environment with a base pressure better than 1.10^{-7} Pa. Layers were deposited at room temperature onto the native oxide of super-polished silicon substrates by physical vapour deposition (electron beam evaporation). Quartz crystal micro-mass balance (QCM) was used to control the amount of deposited material (+/- 1% of the reported values). QCM measures mass change, transferred into nominal layer thickness by calculation. This nominal layer thickness incorporates an amount of material that adds up to this thickness at bulk density (Cu: 8.93 g/cm^3, Au: 19.3 g/cm^3). Amounts (and rates) in this paper are reported based on the nominal layer thickness or thickness change. Copper was deposited at a constant rate that was varied from sample to sample from a value of 0.006 nm/s up to 0.08 nm/s. Gold was deposited at a rate of 0.005 nm/s. The layers were optically characterized by spectroscopic ellipsometry (SE) real-time during deposition (at 10 s/frame, 2 nm wavelength step size). The spectroscopic ellipsometer used in this study was a Woollam M2000 FI with a spectral range of 250-1700 nm and it is used at 55° angle of incidence with respect to the surface normal. The chemical state of the deposited materials was verified in-vacuum with a VG Clamp1 X-ray photoelectron spectroscopy (XPS).

2.2. Ex-situ techniques

Samples were characterized ex-situ with spectroscopic ellipsometry (SE), X-ray photoelectron spectroscopy (XPS), atomic force microscopy (AFM), grazing incidence X-ray diffraction and reflection (XRD/XRR) and secondary electron microscopy (SEM). The AFM's used to characterize the morphology were either a Park NX10 or a Bruker Dimensions used in tapping/ dynamic mode. XPS data were acquired with a VG Clamp1, using non-monochromatic Al Kα. In all presented XPS data a detector pass energy of 75 eV has been used. Secondary electron microscopy images were obtained with a FEI Verios 460 at 10 kV in secondary electron mode. Grazing incidence X-ray diffraction and reflection (Cu Kα) were obtained by a Bruker D8 eco. XRR measurements of thin films can be used to determine film properties like layer thickness and interface roughness, but here they were used to determine the tooling factor of the QCM. Fig. 1 shows an example of XRR measurements for a thick and thin copper film (45 nm and 4.5 nm). The thick film shows a number of oscillations in the theta range of 0.5- 1°. The periodicity of the oscillations can be interpreted via Bragg's law to a layer thickness. For the thin film the number of oscillations is too low to establish an accurate value. The island growth mode of the thin film provides a "rough" film that loses intensity fast for increasing theta in XRR, preventing the higher order Bragg oscillations to show. Film thicknesses in the range of 20 to 50 nm of materials with small amounts of atmospheric oxidation, in our case silicon and copper, were used to determine the QCM tooling factor.

2.3. Ellipsometry

Spectroscopic ellipsometry (SE) is a non-destructive tool to monitor thin film evolution real-time. It is an optical surface analysis technique based on the change of polarisation of light interacting with matter. Interpretation of the data, however, should be done with care, especially for the ultra-thin layers or nano-clusters described in this paper. Although the SE use in this study has an extended spectral range from the visible toward both the ultraviolet and the infrared, linking the optical properties to that of the evolving film is complex at best. The optical properties of the thin film are governed by many factors including inter- and intraband transitions as well as morphology, density and chemical composition.

2.3.1. General

Ellipsometry data is usually expressed in terms of the amplitude ratio ψ and phase angle Δ. These parameters are related to the complex Fresnel reflection coefficients via the complex ellipsometric parameter ρ:

$$\rho=\frac{r_p}{r_s} = \tan(\Psi)\cdot e^{i\Delta} \qquad \text{equation (1)}$$

where r_p and r_s are the complex Fresnel reflection coefficient for p- and s-polarized light. From the ellipsometric data obtained, the dispersion relation of the optical constants over the probed photon energy range can be deduced. In the case of a single opaque substrate, optical properties can be deduces via the pseudo-dielectric function, but more often ellipsometry is used for (thin) films. The optical constants are expressed in the complex refractive index $\underline{n}= n+i.k$ or in terms of the complex dielectric function $\underline{\varepsilon}= \varepsilon 1+i.\varepsilon 2$ of the layers. The latter are related through the definitions $\varepsilon 1=n^2-k^2$ and $\varepsilon 2= 2.n.k$. With photocatalytic applications in mind, light absorption is a key parameter. Therefore $\varepsilon 2$ of the grown films are presented in this paper.

2.3.2. In-situ ellipsometry

In-situ analysis inside a vacuum setup requires to take care of the view ports. Besides ensuring to be transparent for the used spectral range, even dedicated view ports for ellipsometry are never perfectly strain-free. This will mainly manifest in a mismatch in ellipsometer parameter Δ. This effect is a constant factor over time and can be taken into account using an offset. This offset is determined on the bare silicon wafer at time zero. Furthermore, a small ψ mismatch in the spectral range of 4-4.5 eV is remedied by using an effective substrate for the silicon wafer at time zero instead of library silicon optical properties. This mismatch is believed to be a substrate property rather than a view port effect. The optical properties of the "library"-materials that are used in this paper are presented in

Fig. 2. The kink in the data for copper are part of Palik's data [15], since he combined data sets from Dold and Mecke in the infrared (IR) region (0.13–0.98 eV) and data from Hagemann *et al*. in the range of 1 to 5 eV. Further noteworthy is that, although attenuation lengths for optical techniques are usually not surface sensitive, the high absorption values ($\varepsilon 2$) of the silicon substrate ensure that in the region above 3 eV the penetration depth of the incident light in silicon is less than 10 nm. Changes in reflection in this region are therefore very surface sensitive and allow for estimations on the (sub-) nanometer thickness scale.

2.3.3. Ellipsometer and transmission measurements

The ellipsometer modelling procedure described in this paper makes use of ellipsometer in the reflection mode. Another characterization technique often employed to sample optical properties is transmission measurements, usually with UV-Vis spectroscopy. In order to validate the ellipsometer fitting procedure, a 4.5 nm nominal thick copper film has been deposited on a glass substrate. This substrate has been probed by ellipsometer in reflectance and transmission mode as well as with a Perkin Elmer Lambda 1050 UV-Vis-NIR spectroscope with similar spectral range. The transmission measurements have been performed with the bare glass substrate as a reference to obtain the transmission of the copper film. The measurements were performed one day apart on a 1 month atmospheric exposed sample to have the composition in a (more or less) steady state. Fig. 3 shows the results of these transmission measurements as well as the results obtained by modelling the ellipsometer reflectance date of the same sample. All the presented modes produce similar results. The model results from ellipsometer reflectance and ellipsometer transmission measurements match within a few percent. The non-uniform spectral intensity profile of the Xe source of the ellipsometer setup is visible in the noise level of the IR-part of the transmission mode, showing the improved spectral quality when using the reflectance mode. The UV-Vis shows a transmission that is up to 10% higher than the ellipsometer measurements, but the spectral shape of UV-Vis and the model match to a good degree. In most studies the spectral shape is the most interesting. Furthermore the larger discrepancy seems to be between ellipsometer transmission and UV-Vis transmission and not between the two ellipsometer modes.

2.3.4. Model accuracy

In this paper the deposited films do not form a closed layer and a slab model of thin films should be treated with care. In the next section we argue that the B-spline model can be employed for thin films of gold and copper and sketched the boundary conditions. Throughout the paper the metal layers are always modelled with a B-spline and an effective layer thickness as described in section 3.1. The last consideration of this experimental section on ellipsometry concerns the error or accuracy of the presented permittivity data. Many potential errors can influence the outcome of spectroscopic ellipsometry. With the use of a silicon wafer substrate and sufficient averaging time per spectroscopic scan (order of seconds) intensity related errors (stochastic noise) are only a minor part. Only in the periphery of the spectrum (below 1.0 eV and above 4.5eV) this intensity error would account for ~1% relative error of the presented values. By far the biggest contribution is the assumed or calculated value for the effective film thickness. Using the AFM data presented in this paper as a guide, a 10% thickness error is quite realistic. How this would influence the outcome of the B-spline fit in the model is depicted in Fig. 4 where the permittivity result of the B-spline/SiO_2/Si wafer model fit to the spectroscopic data of a 4.5 nm nominal thickness copper film are shown. A different thickness will change the interpretation of the results slightly, but the peak position around 1.85 eV remains at the same position (+/-0.02 eV). Only the amplitude differs. The change in amplitude scales roughly linear to the assume thickness error: amplitude difference of +/-7% for thickness error of +/- 10%. These accuracies are but a fraction of the observed peak shifts and amplitude changes reported in this paper due to changes in amounts or growth/exposure conditions, showing the significance of the results.

2.4. Data analysis

All ellipsometer data was analysed with CompleteEASE software (version 4.64) of J.A. Woollam Co Inc. This paper uses a tailor made fitting procedure for copper and gold nano-clusters that is described in detail in section 3.1. The routine has been established on gold to bypass possible chemical or morphological modifications due to atmospheric exposure or possible complications of monitoring in vacuum. The B-spline fitting routine used here includes Kramers–Kronig consistent dielectric functions to ensure a realistic physical shape of optical properties. Together with the slab layer model, permittivity data have been extracted for all monitored films. All permittivity data result from a fit with a mean square error (MSE) between data and model of 0.1-0.2%. With photocatalytic applications in mind, light absorption is a key parameter and the $\varepsilon 2$ of the grown films are presented in this paper. XPS data was analysed by CasaXPS (version 2.3.16). Finally, morphology images of AFM and SEM were analysed with Gwyddion software (version 2.41).

3. Results and discussion

Within the used spectral range (in this paper 250-1700 nm) it is usually possible to extract the optical performance of the film under observation [16-22], including potential interaction with reactive environments. For thin copper films spectroscopic ellipsometer has already been employed to investigate the conductive properties for electrical inter-connect applications [23]. This study however focuses on copper nano-clusters below the percolation limit where surface conductivity is absent. The copper nano-clusters are used to explore the potential of spectroscopic ellipsometry both in-situ and ex-situ.

3.1. Ellipsometry of copper

Copper is deposited at room temperature to allow for Volmer-Weber growth of insulated copper islands. The deposited quantity is chosen to keep the copper clusters within the nanometer size range (diameter smaller than 20 nm). Significant off-specular scattering effects are not expected. Although the rest of this paper will convert the ellipsometer data into permittivity, already the ellipsometer amplitude ratio ψ and phase angle Δ can be informative. Fig. 5 shows two frame from in-situ ellipsometer data of copper growth. The substrate data is taken at time zero before any deposit has reached the silicon substrate and the data labelled Cu (4.5) was taken after the copper deposition was stopped at 4.5 nm film thickness on the QCM. Furthermore, a modelled curve is plotted indicating the expected ellipsometer parameters for the same quantity of copper using library (Palik) constants. The difference between bare substrate and copper deposit is apparent. For the spectral range of the metals interband region (typically above 2.1 eV), the slab model using bulk copper properties is describing the data reasonably well: where amplitude ratio ψ is still showing a difference, the phase angle Δ is covered reasonably well. Generally, phase angle Δ is more indicative for the thin film's thickness, were amplitude ratio ψ is more indicative for the optical properties of the thin film. The largest discrepancy between model and copper measurement is to be found in the region below 2.1 eV. Here the model shows the characteristic rise of amplitude ratio ψ when going towards the infrared due to the Drude absorption of bulk copper. The measured data, on the other hand, returns to the substrate values in the spectral range below 1 eV. The absence of this Drude term, or in other words, this transparency in the intraband region of copper, is indicative for *plasmon excitations* of copper. Before discussing the intraband in more detail, the ellipsometer parameters ψ and Δ need to be modelled to be useful in discussing possible *plasmon excitations*. The next sub-sections are dedicated to the modelling of ellipsometer data presented in this paper.

3.1.1. Modelling ellipsometer data

The most straight-forward interpretation of ellipsometer data is the case of a single opaque substrate. The optical properties can now be deduces via the pseudo-dielectric function [19]. To verify both the optical properties of our copper deposit and the applicability of Palik's "library"-values, we deposited a 45 nm thick copper film analogue to Haidu *et al*. [23]. The result for the thick copper film is shown in Fig. 6. The measured data is plotted in open circles to illustrate both the point density and to indicate the stochastic noise level of the measurements (size of the circles). The solid curves present a Drude term that fits the intraband region of Palik in the 1-5 eV range, the interband region from Palik and the sum of the intra- and interband. The Drude term is a fit to Hagemann *et al.*'s part of Palik's data with a plasma frequency of 8.5 eV and a dampening constant of 0.13. This is slightly different from the 8.8 eV and 0.105 values reported by Oates *et al.* [19], but is in line with the range reported by Haidu *et al.*[23]. The plotted Drude term in Fig. 6 is a good match to our copper data in the infrared region (0.7-1.5 eV). Furthermore, the interband region also presents a good match to our copper data. We are producing the same copper optical properties for an opaque film as literature.

3.1.2. EMA vs. B-spline on gold

The properties of relatively thick copper layers are not the topic of this paper; the behaviour of these films are adequately described by Haidu *et al.* This paper focusses on the region where copper is not showing a significant Drude term and *plasmon resonance* effects occur. Usually this regime is governed by insulated clusters/ islands that form a 3D landscape. The Volmer-Weber island growth regime for quantities below the percolation limit used here produces nano-cluster much smaller than the wavelengths used to probe them. How to deal with these (extremely) rough thin films is topic of this section.

To bypass complications of in-situ measurement and corrosion/ modification by atmospheric exposure, we used ultra-thin gold films to establish an appropriate ellipsometer fitting routine for our 3D landscapes. Gold as well as copper evolves with Volmer-Weber island growth and the optical properties of gold and copper are similar. The characterization of the thin gold film were performed ex-situ. Gold, being more noble than copper, remains unaffected by exposure to atmosphere, making in-situ and ex-situ characterization interchangeable.

Haidu *et al.* propose a Bruggemann effective medium approach (EMA) to resolve data below the percolation limit. An EMA is usually used to model the roughness of the top of a thin film when this rough top is only a fraction of the total film thickness. Typically a void fraction of 50% and a depolarization factor of 0.33 (indicating spherical inclusions) will provide a decent fit. For the landscape under consideration here, this typical approach is resulting in a poor fit. Below is described how the EMA needs to be modified. For gold, Beyene *et al.* [16] propose a Kramers-Kronig consistent B-spline fit method for systems similar to ours. We have tried both the EMA and B-spline models on our data for a 3 nm (QCM) nominal thick gold film. Fig. 7 shows ellipsometer angles ψ and Δ as well as $\varepsilon 2$ from both models. The plot of the ellipsometer angles also shows the spectra of the bare silicon surface. The difference with the small quantity of gold is apparent. To show the fit quality, the data is plotted in data points with a circle diameter of approximately two times the stochastic noise level of the used settings. The models are plotted in solid lines. Both the EMA and the B-spline fit model produce a reasonable (EMA) to good (B-spline) fit to the data. This is usually reported as mean square error (MSE) of the model to the data. The plotted EMA-model shows a MSE of 0.72% whereas the B-spline shows a MSE of 0.16%. The difference in fit quality of the two models mainly manifests in the region below 2.5 eV; the region of interest of this paper. The presented EMA is a mix of 25% void and 75% gold (Palik). Furthermore, similar to Haidu, the depolarization factor in the Bruggemann effective medium needs to be tuned to 0.88 (indicating an oblate spheroid shape of the gold). This might actually be a reasonable description of the 3D gold landscape. On the other hand, the fit quality difference with the B-spline model is considerable. Both models are however predicting the interband region adequately as is shown in the plot of $\varepsilon 2$ where Palik's interband data for gold are plotted.

In order to be able to use the good fit quality of the B-spline model we have to overcome one weakness of this model: it has a poor link to a physically meaningful layer thickness. Detrimental for the B-spline model is the effective film thickness assumed (or attempted to fit). In order to establish a routine suited for the 3D landscapes we intent to investigate, the next section details the approach to extract meaningful optical properties from ellipsometer data only. This will be prerequisite when materials are investigated that are not invariant for in-situ and ex-situ characterization, as is the case for copper.

3.1.3. Detailed Ellipsometer fitting routine

The ellipsometric parameters can be used on their own as is shown in Fig. 5 or Fig. 7, but to extract most information they are converted in optical properties of the thin film. In this paper the dielectric function of a film ($\varepsilon 2$) is a direct measure of its absorbance. In order to establish a routine to extract a meaningful effective film thickness from ellipsometer data, different quantities of gold have been prepared and analysed ex-situ both with ellipsometer and atomic force microscopy.

Fig. 8 depicts the effective film thickness versus nominal film thickness (QCM) determined in two different ways. The first (labelled ellipsometer) makes use of (part of) spectroscopic ellipsometer data, the second uses atomic force images (AFM). From the spectroscopic ellipsometer data the part of the spectrum is used that is not affected by possible contribution of the Drude term nor by *surface plasmon resonance* effects of gold. Using the interband optical constants of gold from Palik [15] in a spectral range of 3.5–5 eV an effective film thickness can be fitted using an optical slab model of parallel layers for substrate and overlayer. This enables to have a current effective film thickness for every ellipsometer measurement or at every frame of an in-situ measurement. The second approach (labelled AFM) uses atomic force images of the gold films. From the images the partial coverage of the substrate is apparent (30%-60%). With the lateral dimensions of the clusters of the same order as the probe diameter, extracting an exact coverage from AFM images is difficult at best and involves decomposing island and probe shape. The individual island height above the substrate level can however be measured by AFM to a very high degree of accuracy due to the partial coverage. The effective thickness for AFM plotted in Fig. 8 is the average maximum height of several hundred up to one thousand clusters (islands) found in a 1 μm x 1 μm size image. The vertical error bar in the AFM data of Fig. 8 indicate the standard deviation of the island's maximum height distribution. The horizontal error indicated the accuracy of the deposited amounts. Fig. 8 shows that the ellipsometry determined effective film thickness matches well with the AFM determined effective film thickness in the nominal film thickness range presented. The effective film thickness thus determined is now fixed and used to interpret the spectroscopic ellipsometer data over the complete range with a B-spline model fit. The B-spline fit in Fig. 7 has been determined in this fashion. The resulting dielectric function of the film ($\varepsilon 2$) looks very similar to the results presented by Beyene *at al*. [16], who proclaimed it to be the gold nano-cluster plasmonic activity.

Furthermore Fig. 8 shows that for nominal film thickness (QCM) up to 4 nm the effective layer thickness can be more than two times as large as the nominal film thickness, not necessarily scaling linear with deposited amounts

(= QCM value). This is a trend that is also observed when effective film thickness is estimated with an EMA as presented in section 3.1.2. Where our method calculates an effective film thickness of 7 nm for the gold film the EMA calculates a 6.5 nm film thickness with a 25% void fraction. This is still more than a factor 1.5 larger than the QCM value.

To interpret the ellipsometer data of the copper deposits in the intraband as *plasmon excitations* of insulated copper nano-clusters, the morphology landscape is investigated in the next section.

3.2. Nano-cluster size and shape

In order to confirm *plasmon excitations* of copper nano-clusters, three copper film have been prepared with the same quantity of deposit (4.5 nm nominal film thickness), but at significantly different deposition rates. The texture of the samples has been probed by secondary electron microscopy (SEM) and are depicted in Fig. 9. The 250 nm x 250 nm size images of the three copper films show similarly shapes clusters although small differences can be observed. All images show a partial coverage of the substrate (60-70% covered) and (very) small, insulated islands down to 10 nm diameter. Fig. 9 shows that the largest number of clusters and the most narrow size distribution is observed for the lowest rate. Many of the larger clusters, especially in Fig. 9 b) and c) exhibit an asymmetric shape that looks to be composed out of several of the smaller clusters observed. This process is usually called coalescence of clusters during growth. Coalescence is most prominent at the largest growth rate.

In order to quantify this observation, the footprints of the clusters observed in the SEM images of Fig. 9 have been analysed. Island footprints are estimated by making contour maps of the half-maximum-intensity (Gwyddion software). In order to categorize the nano-cluster footprint, the observed area is translated into an equivalent disc radius. This is a reasonable assumption for the cluster shapes of Fig. 9 a), but less so for the larger growth rates displayed in Fig. 9 b) and c) where more elongated shapes are present. Fig. 10 a) shows the statistics obtained from 500 nm x 500 nm size SEM images of which the frames in Fig. 9 are fractions. The curves through the data points serve as guide to the eye. Only at the lowest growth rate (0.006 nm/s) the area distribution shows a single Gaussian shape with an average radius of 9 nm and a sigma of 2.5 nm. With increasing growth rate the main peak of the distribution shifts slightly in position towards 12 nm and broadens significantly up to a 7 nm sigma value. Furthermore, at higher growth rates populations start to appear at radii that are much larger than the average of the main peak (9-12 nm). At the highest growth rate (0.08 nm/s) a significant population is observed at a radius as large as 42 nm. Although the details might differ, all samples presented in Fig. 9 show insulated nano-clusters.

With the amount of deposited material of the frames in Fig. 9 and 10 being the same (based on QCM +/- 1%), the differences in the observed optical response is caused by nano-cluster size and shape together with the small inter-cluster distances [8]. The permittivity extracted from the in-situ ellipsometer data of the three samples of Fig. 9 are displayed in Fig. 10 b). All three samples show a strong absorption peak just below 2 eV in copper's intraband region. Since all three samples show insulated nano-clusters, this absorption is caused by *plasmon excitations*. For the lowest growth rate, the dielectric function ($\varepsilon 2$) and shape (SEM footprint) are described by a single Gaussian distribution. Copper nano-clusters of 9 (+/- 2.5) nm radius and average height of 8 (+/- 1) nm (see AFM in section 3.3.1) exhibit *plasmon excitations* at 1.85 (+/- 0.35) eV. The nano-cluster shape and size arise from self-organisation of the deposited material of which the dimensions can be described by self-similar growth of polycrystalline films [24]. If the dimensions and the shape of the copper nano-clusters are known at every step of the growth, the plasmon resonance position and resonance width can be correlated to an average cluster size and size distribution. The scaling of copper nano-clusters is however beyond the scope of this paper.

For the larger growth rates both dielectric function and shape are not governed by a single Gaussian distribution. The increased amplitude at low photon energy (below 1 eV) and broadening of the optical response with increasing growth rate in Fig. 10 b) is most likely caused by the coalescence of smaller clusters into larger nano-clusters (size typically above 40 nm diameter). If the deposited amount of material is increased beyond the 4.5 nm nominal film thickness, this coalescence process will eventually be responsible for the Drude absorption observed in the bulk layer optical response. For the largest growth rate reported here this percolation limit has been observed to be at a nominal layer thickness of 10 nm. This is a well-studied regime where copper films start to become conductive and where ellipsometry already has proven its use [23].

Furthermore, the increased resonance amplitude value of $\varepsilon 2$ at larger growth rate in Fig. 10 b) shows that the film absorption increases. Combining this with the above observations of island shape and size, it can be concluded that for the same amount of material in-plane larger clusters are more efficient in absorbing light. The stronger effect of larger nano-clusters is consistent with small particle broadening as described by Oats et al. [19]. AFM

measurement of the samples of Fig. 9 show similar height scales (give or take 10%), indicating that the main difference of the systems is in-plain and is captured by the SEM statistics presented above. The different optical responses of the systems in Fig. 10 b) are therefore an example on the sensitivity of ellipsometer data for small changes in texture.

3.3. Copper nano-clusters: material characterization

Material characterization is paramount in interpreting the presented ellipsometer data. Many material characterization techniques are employed ex-situ, allowing interaction with the atmosphere. For copper nano-clusters this poses the challenge of a system that changes composition over time. In order to focus the final part of the paper on spectroscopic ellipsometry, the material characterization is discussed extensively in this section.

3.3.1. Island morphology and height

Besides the SEM characterization presented in section 3.2, copper samples have been investigated by AFM. With the expected amount of copper oxidation to be smaller than a layer of 1 nm (see section 3.3.2), the influence of this on the presented morphology pictures is minimal. Fig. 11 shows an AFM image of a 4.5 nm nominal thickness copper film grown at 0.006 nm/s. The nano-scale copper clusters as well as the partial coverage of the substrate are clearly observed. Furthermore, an average island height of 8 nm is observed which matches the effective layer thickness for the copper layer extracted from ellipsometer data. Looking at the lateral correlation length from the height-difference-correlation plot (called HHCF in the Gwyddion software), a value of 6 nm is observed, showing the nanoscale of the clusters. AFM of the other two 4.5 nm nominal thickness copper films, growth rates 0.02 and 0.08 nm/s, show similar height scales (give or take 10%). With the lateral correlation length in the same order of magnitude as the expected AFM probe radius, exact lateral dimensions cannot be extracted. For probing the lateral dimensions this paper therefore uses SEM images. The individual maximum cluster height however can be determined with AFM to a very high degree of accuracy (usually better than 0.1 nm).

3.3.2. X-ray photoelectron spectroscopy

In order to assess the chemical composition of the nano-clusters, XPS measurements are performed in vacuum before and after copper deposition. Furthermore, copper deposits are measured as deposited and after exposure to atmosphere. All measurements have been performed with the VG Clamp1, using non-monochromatic Al Kα. Fig. 12 shows the survey spectra of the silicon substrate before and after 4.5 nm copper deposition in vacuum. A strong copper signal can be seen in the red curve of the copper deposit. Characteristic copper photoelectron peaks can be observed around 933 eV, but also the lower intensity peaks around 123 eV and 75 eV are observed. Furthermore, the Auger LMM peaks between 650 and 720 eV are clearly seen. Although not very apparent at this magnification, the Si2p and Si2s peaks from the substrate are also clearly visible around 100 eV and 150 eV respectively. The spectrum of the bare silicon wafer only show the silicon peaks. Both scans show a small amount of (most likely) adventitious carbon. Both surveys are quantified by estimating the relative peak intensities and corrected for material specific sensitivities using the Scofield library. The results are plotted in Table 1. These results show the in vacuum copper deposit to be in the metallic state. The copper peak position matches with the metallic state. Furthermore, the amount of oxygen observed is too low to consider cuprite (Cu_2O). The observed oxygen concentration in the survey of the copper deposit originates mainly from the native oxide of the silicon wafer. This can be conclude from the similar O1s/Si2p ratios for both the bare substrate and the copper deposit as well as the O1s peak position.

XPS: atomic concentration [%]

	pre	Cu(4.5 nm)
Si2p	44	14
C1s	14	6
O1s	42	11
Cu2p3	0	69

Table 1: In-vacuum XPS quantification results before (pre) and after copper deposition (Cu).

This copper deposit was extracted from the vacuum setup and exposed for 7 days to atmospheric conditions. The resulting Cu2p XPS scans are depicted in Fig. 13. In order to compare the in vacuum with the exposed copper, the intensity of the deposited copper is scaled down to match that of the exposed copper. Where the as deposited

copper shows the typical shape for metallic copper, the exposed sample shows two contributions to the Cu2p. For the $Cu2p_{3/2}$ peak this two contributions are indicated by the dashed curves. The larger intensity part is at copper's metallic position, whereas the smaller intensity part is at copper in the Cu^{2+} position of CuO or $Cu(OH)_2$. Furthermore, the additional broad peak around 943 eV is indicative for Cu^{2+}. With the used XPS setup it is not possible to distinguish between copper in the metallic or copper in the Cu^{1+} state of cuprite (Cu_2O). The crystal state of the main intensity of the exposed copper will be discussed in the next section, where XRD provides the final verdict on the main copper intensity of the XPS measurement of the exposed copper.

Besides providing input for atomic concentration tables, quantified XPS results can be employed in a single overlayer algorithm assuming an overlayer A and a substrate layer B. Using a derivative of the Beer-Lambert law, the thickness, t, of the overlayer can be calculated:

$$t = \frac{AL.\ln\left[1+K.\frac{I(A)}{I(B)}\right]}{\cos(\theta)} \qquad \text{equation (2)}$$

With AL the attenuation length (for Cu2p the AL= 0.8 nm), K the atomic density ratio substrate/ overlayer (and sensitivity factors if applicable), I(A) and I(B) the peak intensities of overlayer and substrate layer and θ the emission angle (for this setup 0°). The dashed curves in Fig. 13 show the decomposition of the exposed copper peak in a metallic (the larger intensity) and an oxide part. Assuming the oxide to be the overlayer, the intensity ratio of 0.23 would be accounted for by about 0.3 nm thick CuO at a density of 6.4 g/cm^3. This overlayer model is only accurate for flat films. The morphology of the thin copper film cannot be considered flat according to the AFM image of Fig. 11. Due to this roughness the 0.3 nm CuO layer thickness value will have a large relative error of +/- 50%. It serves to illustrate that a shoulder in the Cu2p peak can be caused by a small quantity of the initial amount: roughly one monolayer of the original copper film.

3.3.3. Grazing angle X-ray diffraction

To identify the state of the copper after atmospheric exposure, grazing incident X-ray diffraction is employed (XRD). The Cu Kα XRD spectrum of two samples deposited in the same setup are taken at a fixed source angle of 1°. Fig. 14 shows a thick copper film (nominal thickness 45 nm) and a thin copper film (nominal thickness 4.5 nm) after one day of atmospheric exposure. The coloured bars in Fig. 14 indicate the main peaks of library positions and their relative intensities of cubic copper in a metallic state (red), cubic Cu^{1+} of Cu_2O (green) and monoclinic Cu^{2+} of CuO (blue). The broad peak around a 2theta of 55° is caused by the crystal lattice of the silicon substrate not being rotated completely out of view. The spectrum of the thick copper film is matching the metallic texture with the strongest peak in the (1,1,1) direction around 43°. The thin copper film shows only one peak: a peak around 43°. This matches only with the metallic texture. From the width of the diffraction peaks information on the average grain size, d, in that direction can be extracted. This employs the Scherrer equation:

$$d = \frac{K.\lambda}{\Delta(2theta).\cos(\theta)} \qquad \text{equation (3)}$$

With dimensionless shape factor K (0.94 for polycrystalline films), the X-ray wavelength of Cu Kα (λ= 0.1504 nm), Δ(2theta) the fwhm in units of 2theta corrected for an instrumental broadening of 0.25° and θ the Bragg angle of the peak. The average grain size in the (1,1,1) direction for the thick copper film is 46 nm, whereas the thin film shows a size of 7 nm. The XRD spectrum of the thin film show the copper to be in a metallic state with a grain size of approximately the effective film thickness used in ellipsometer modelling. This supports the claim that this paper studies nano-clusters of mainly metallic copper with a small, but significant, modification due to atmospheric exposure.

3.4. In-situ growth of copper nano-cluster

In this section we are going to analyse the in-situ data of *plasmon excitations* in metallic copper nano-clusters in detail. With the effective film thickness determined by in-situ ellipsometry as described above, a Kramers-Kronig consistent B-spline model fit on the full spectral range results in the permittivity ($\varepsilon 2$) plotted in Fig. 15. The labels in Fig. 15 a) indicate the nominal film thickness as monitored on the QCM in nanometers. The nano-clusters in Fig. 15 are grown at a rate of 0.006 nm/s. The dashed line in Fig. 15 a) is the interband permittivity of copper according to Palik's data. If a *plasmon resonance* would be absent for the insulated nano-clusters under observation, the permittivity would be similar to bulk copper's interband. For thickness values below 1 nm no clear difference can be observed in the intraband region of copper, either because the nano-clusters for this amount do not show *plasmon resonance*, but more likely because the resonance effect overlaps and is overshadowed by copper's interband behaviour.

At larger amounts the permittivity ($\varepsilon 2$) is showing a clear difference from copper's interband with a *plasmon resonance* around 2 eV. Fig. 15 b) shows the resonance peak position and amplitude at different thickness. This position and amplitude are determined by the energy and values of the maximum position observed in $\varepsilon 2$. With (most of) the positions below copper's bandgap, no interband contribution is expected in this maximum value. The resonance is both increasing in amplitude and red-shifting with increasing film thickness. The position shifts linearly from 2.10 eV at a nominal film thickness of 1.2 nm down to 1.85 eV at a nominal film thickness of 4.5 nm. The amplitude of the *plasmon excitation* increases linearly with the deposited amount as well. From an amplitude of 5 at a nominal film thickness of 1.2 nm up to 15 at a nominal film thickness of 4.5 nm. When parameterized by Gaussians, the main peak turns out to mainly shift at a constant width, indicating that all copper nano-clusters increase in size with an approximately constant size distribution. These in-situ ellipsometer results show that the self-organisation of copper growth can be used to create nano-clusters with tuneable *plasmon excitations*, highly interesting for photocatalytic applications. The interband regions for the copper deposits (above 2.1 eV) also show differences with respect to Palik's interband. Although ellipsometer can in principle be used to extract details of the interband, in this paper this region is used to establish an effective layer thickness for modelling. The detailed shape is critically depending on the exact value for this thickness and remains open for debate. The effect of an effective layer thickness error has been presented in the experimental section.

The exact shape and position of this *plasmon excitations* depends on the deposition conditions. Changing growth conditions like growth temperature or deposition rate can induce (large) differences in nano-clusters size, shape and density. The different rates presented in Fig. 10 b) have been monitored in-situ as well and show similar behaviour to the rate presented in Fig. 15: linear increase of resonance position and amplitude of the resonance around 2 eV. The do however show additional peaks appearing at significantly lower (typically around 1 eV) photon energy. With increasing amounts these lower energy resonance peaks will overshadow the resonance around 2 eV and ultimately become the Drude absorption know from bulk metal (i.e. a resonance at zero photon energy).

3.5. Nano-cluster oxidation

In the controlled environment of the UHV-setup the metallic nature of the copper nano-cluster surface remains intact and in-situ ellipsomety can extract the optical properties of metallic copper. Ex-situ spectroscopic ellipsometry is equally important to understand the sensitivity of the technique to chemical modifications. As soon as metallic copper is exposed to atmosphere, oxidation takes place [11-13]. This will be of consequence for catalysis applications and also has its effect on the optical performance of the nano-clusters. A thin layer of approximately 0.3-1 nm thickness of copper-oxide is formed on the copper clusters upon exposure to atmosphere [25]. This small amount will not affect the ellipsometer parameters of the thin film significantly using copper-oxide optical constants (from Palik, [15]) to calculate the response for a slab-model CuO/copper. It will however affect the *plasmon excitations.* The metal-oxide layer can act for example as a higher than air refractive index shell around the nano-clusters or it can change the size or shape of the nano-clusters. *Plasmon excitations* are highly sensitive to both.

In order to assess the optical effect of a thin metal-oxide covering layer, the native oxide layer (most likely CuO) on a 4.5 nm nominal thickness copper film is compared to the metallic state. The native oxide layer will form when the film is extracted from the UHV setup and exposed to atmosphere. XPS measurement shows that after a week exposure to atmospheric conditions only a 0.3 nm thick CuO layer (roughly one monolayer of the original copper film) is present together with the metallic copper [11, 12, 26, 27]. Fig. 16 a) shows the permittivity ($\varepsilon 2$) after different exposure time together with the permittivity of the metallic-state. Given the small amount of copper-oxide, ellipsometer modelling has used the same effective film thickness for all measurements. Fig. 16 b) shows the resonance position and amplitude of the exposed samples at different exposure time. The axis maxima of Fig. 16 b) have been set to the values of the metallic state. The first ex-situ time (~15 minutes) is almost instantly measured after vacuum extraction. This exposure time is already sufficient to red-shift the *plasmon resonance* for 0.2 eV. This is half of the 0.4 eV (= 180 nm wavelength) observed after 1 week. Where the metallic state has a resonance with a red coloured appearance (~660 nm wavelength), the atmospheric exposure shift the film colour beyond the visible range. The amplitude of the resonance shows an even more extreme behaviour. The first ex-situ time (~15 minutes exposure) already is responsible for an amplitude drop of 4 out of the 5 in permittivity loss after 1 week exposure. After this initial drop, the amplitude seems to drop slowly but steadily about linear with exposure time. This last slow decay is not accompanied by a red-shift, since the resonance positions at 1 day and 1 week of exposure are almost identical. The relatively fast amplitude decay and red-shift in the first day is believed to be related to the oxidation of the first monolayer of the metallic copper nano-clusters. Whether this is because

of the CuO shell surrounding the nano-cluster or because the space between nano-clusters is modified remains to be resolved.

4. Conclusion

The Volmer-Weber growth of copper deposits below the percolation limit exhibit *plasmon excitations.* The deposits show the potential of spectroscopic ellipsometry to probe the optical properties of plasmon active material. It combines the in-situ capacity of ellipsometry with its excellent sensitivity to *plasmon excitations* within the visible part of the solar spectrum. Furthermore, the self-organisation of copper growth can be used to create nano-clusters with tuneable *plasmon excitations*, highly interesting for photocatalytic applications.

Real-time measurements of copper in its metallic state show a significant *plasmon resonance* contribution to ellipsometer data for amounts above 1 nm nominal film thickness. Furthermore, in this paper the resonance position can be tuned in the range of 1.85-2.1 eV (wavelength difference of 80 nm) depending on the deposited amount. The amplitude of this resonance increases from a value of 5 up to a value of 15. This tuneable resonance can be used to advance photo-catalytic application by selecting the spectral location and strength of light absorption. Spectroscopic ellipsometry furthermore exhibits good sensitivity to ultra-thin (down to sub-nanometer thick) metal-oxide shells covering the copper nano-clusters. Studying the exposure to atmosphere of copper nano-clusters, it is shown that *plasmon resonance* red-shifts almost instantly (0.4 eV/ 180 nm wavelength) after one day of exposure. The amplitudes are reduced in intensity significantly (factor 1.5 compared to the metallic state).

As is the case more often than not, interpreting changes in spectroscopic ellipsometry should be done with care and, where possible, with a variety of (surface sensitive) techniques. Providing this, we have shown that when investigating systems that show *plasmon excitations* near the visible wavelength range, the spectroscopic ellipsometer technique can monitor very small changes of both chemical and morphological nature. This presents opportunities in real-time monitoring in gaseous or liquid environments.

Acknowledgements

I would like to acknowledge Jan Verhoeven (ARCNL, the Netherlands) for his continuing support in generating new ideas and promoting to report on older ones. Furthermore, Erik Langereis (DIFFER, the Netherlands) has help me a lot by discussing ellipsometery in general and the critical reading of this manuscript. Anna Meshkova (DIFFER/Fuji, the Netherlands) has provided me with beautiful AFM pictures of gold. Finally Hans Zeijlemakers (AMOLF, the Netherlands) made possible the detailed measurements of the films with SEM. DIFFER is part of the Netherlands Organisation for Scientific Research (NWO).

References

[1] I. Freestone, N. Meeks, M. Sax, C. Higgitt, The Lycurgus Cup - A Roman nanotechnology, Gold Bulletin, 40 (2007) 270-277.
[2] H.A. Atwater, A. Polman, Plasmonics for improved photovoltaic devices, Nature Materials, 9 (2010) 205-213.
[3] M.L. Brongersma, N.J. Halas, P. Nordlander, Plasmon-induced hot carrier science and technology, Nature Nanotechnology, 10 (2015) 25-34.
[4] C. Clavero, Plasmon-induced hot-electron generation at nanoparticle/metal-oxide interfaces for photovoltaic and photocatalytic devices, Nature Photonics, 8 (2014) 95-103.
[5] S. Linic, P. Christopher, D.B. Ingram, Plasmonic-metal nanostructures for efficient conversion of solar to chemical energy, Nature Materials, 10 (2011) 911-921.
[6] I. Thomann, B.A. Pinaud, Z. Chen, B.M. Clemens, T.F. Jaramillo, M.L. Brongersma, Plasmon Enhanced Solar-to-Fuel Energy Conversion, Nano Letters, 11 (2011) 3440-3446.
[7] J.A. Schuller, E.S. Barnard, W. Cai, Y.C. Jun, J.S. White, M.L. Brongersma, Plasmonics for extreme light concentration and manipulation, Nature Materials, 9 (2010) 193-204.
[8] J.M. Sanz, D. Ortiz, R. Alcaraz de la Osa, J.M. Saiz, F. Gonzalez, A.S. Brown, M. Losurdo, H.O. Everitt, F. Moreno, UV Plasmonic Behavior of Various Metal Nanoparticles in the Near- and Far-Field Regimes: Geometry and Substrate Effects, Journal of Physical Chemistry C, 117 (2013) 19606-19615.

[9] K.M. Pan, H. Ming, H. Yu, Y. Liu, Z.H. Kang, H. Zhang, S.T. Lee, Different copper oxide nanostructures: Synthesis, characterization, and application for C-N cross-coupling catalysis, Crystal Research and Technology, 46 (2011) 1167-1174.
[10] L. Armelao, D. Barreca, G. Bottaro, A. Gasparotto, S. Gross, C. Maragno, E. Tondello, Recent trends on nanocomposites based on Cu, Ag and Au clusters: A closer look, Coordination Chemistry Reviews, 250 (2006) 1294-1314.
[11] K. Fujita, D. Ando, M. Uchikoshi, K. Mimura, M. Isshiki, New model for low-temperature oxidation of copper single crystal, Applied Surface Science, 276 (2013) 347-358.
[12] J.-W. Lim, J. Iijima, Y. Zhu, J.H. Yoo, G.-S. Choi, K. Mimura, M. Isshiki, Nanoscale investigation of long-term native oxidation of Cu films, Thin Solid Films, 516 (2008) 4040-4046.
[13] J. Sancho-Parramon, B. Okorn, K. Salamon, V. Janicki, Plasmonic resonances in copper island films, Applied Surface Science, 463 (2019) 847-853.
[14] B. Sinha, T. Goswami, S. Paul, A. Misra, The impact of surface structure and band gap on the optoelectronic properties of Cu2O nanoclusters of varying size and symmetry, RSC Advances, 4 (2014) 5092-5104.
[15] E.D. Palik, Handbook of Optical Constants of Solids, Academic Press, 1998.
[16] H.T. Beyene, J.W. Weber, M.A. Verheijen, M.C.M. van de Sanden, M. Creatore, Real time in situ spectroscopic ellipsometry of the growth and plasmonic properties of au nanoparticles on SiO2, Nano Research, 5 (2012) 513-520.
[17] T.W.H. Oates, Real time spectroscopic ellipsometry of nanoparticle growth, Applied Physics Letters, 88 (2006) 213115.
[18] T.W.H. Oates, L. Ryves, M.M.M. Bilek, Dielectric functions of a growing silver film determined using dynamic in situ spectroscopic ellipsometry, Optics Express, 16 (2008) 2302-2314.
[19] T.W.H. Oates, H. Wormeester, H. Arwin, Characterization of plasmonic effects in thin films and metamaterials using spectroscopic ellipsometry, Progress in Surface Science, 86 (2011) 328-376.
[20] M. Schwartzkopf, G. Santoro, C.J. Brett, A. Rothkirch, O. Polonskyi, A. Hinz, E. Metwalli, Y. Yao, T. Strunskus, F. Faupel, P. Muller-Buschbaum, S.V. Roth, Real-Time Monitoring of Morphology and Optical Properties during Sputter Deposition for Tailoring Metal-Polymer Interfaces, Acs Applied Materials & Interfaces, 7 (2015) 13547-13556.
[21] P.C. Wu, M. Losurdo, T.H. Kim, O. Choi, G. Bruno, A.S. Brown, In situ spectroscopic ellipsometry to monitor surface plasmon resonant group-III metals deposited by molecular beam epitaxy, Journal of Vacuum Science & Technology B, 25 (2007) 1019-1023.
[22] E. Langereis, S. B S Heil, H. C M Knoops, W. Keuning, M.C.M. Sanden, W.M.M. Kessels, In situ spectroscopic ellipsometry as a versatile tool for studying atomic layer deposition, Journal of Physics D: Applied Physics, 42 (2009) 073001.
[23] F. Haidu, O.D. Gordan, D.R.T. Zahn, In situ ellipsometric study of copper growth on silicon, Thin Solid Films, 520 (2012) 4410-4417.
[24] C.V. Thompson, Structure Evolution During Processing of Polycrystalline Films, Annual Review of Materials Science, 30 (2000) 159-190.
[25] T. Tsarfati, E. Zoethout, R. van de Kruijs, F. Bijkerk, Growth and sacrificial oxidation of transition metal nanolayers, Surface Science, 603 (2009) 1041-1045.
[26] D. Briggs, J.T. Grant, Surface Analysis by Auger and X-ray photoelectron spectroscopy, IMPublications and SurfaceSpectra, Chichester, UK, 2003.
[27] E. Zoethout, E. Louis, F. Bijkerk, In depth study of molybdenum silicon compound formation at buried interfaces, Journal of Applied Physics, 120 (2016) 115303.

Figures and Captions

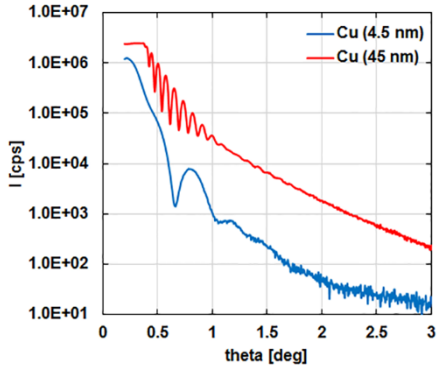

Fig. 1: XRR of 45 nm and 4.5 nm copper.

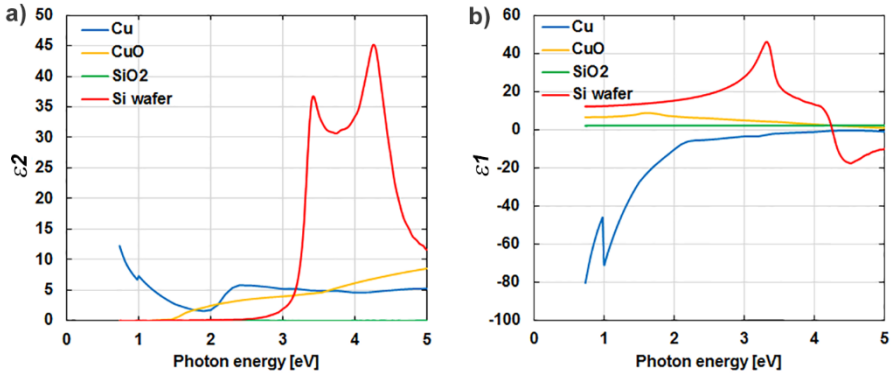

Fig. 2: Used optical constants in modelling of ellipsometer data.

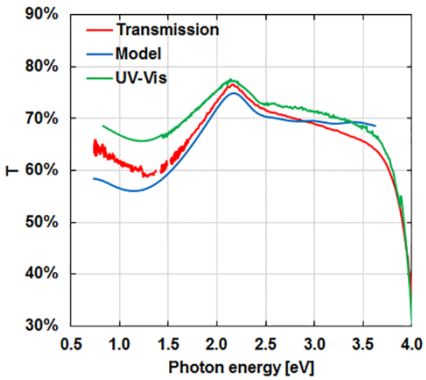

Fig. 3: UV-Vis and ellipsometer data of 4.5 nm copper on a glass substrate in transmission. The model spectrum results from reflectance ellipsometer measurement and B-spline modelling on the same sample.

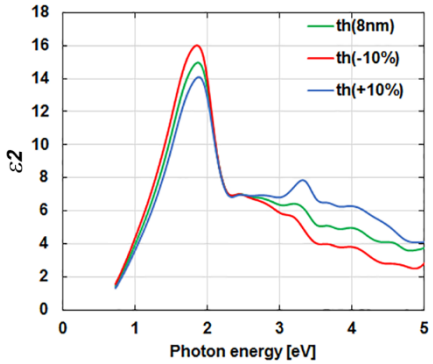

Fig. 4: Permittivity result of ellipsometer slab layer model B-spline/SiO_2/Si wafer of a 4.5 nm nominal thickness copper film. Main factor for error estimation is the effective layer thickness used for the B-spline.

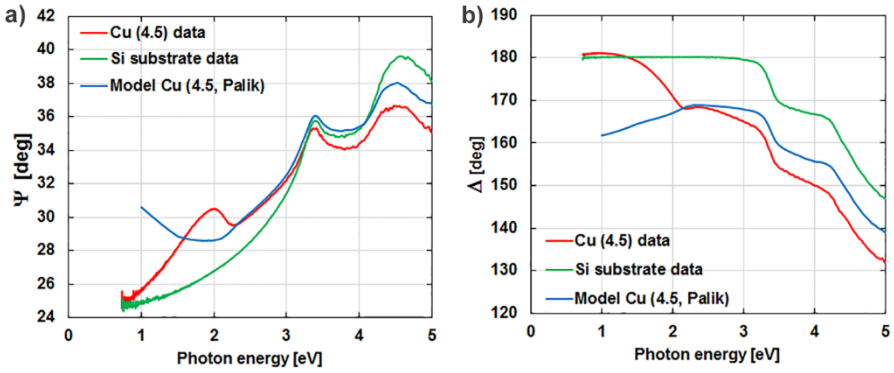

Fig. 5: Ellipsometer parameters Ψ and Δ of in-situ ellipsometer data for 4.5 nm (QCM) thick copper, the bare silicon substrate and modelled data of the 4.5 nm thick copper with Palik's optical properties. The copper was grown at a rate of 0.006 nm/s.

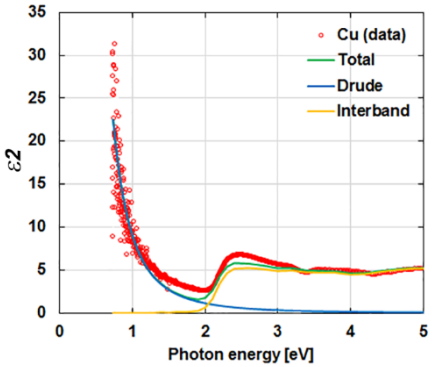

Fig.6: Pseudo-potential results of 45 nm thick copper. Data points are indicated by open circles. The Drude model fits to Palik's copper data and the interband line comes from the optical data of Palik as well.

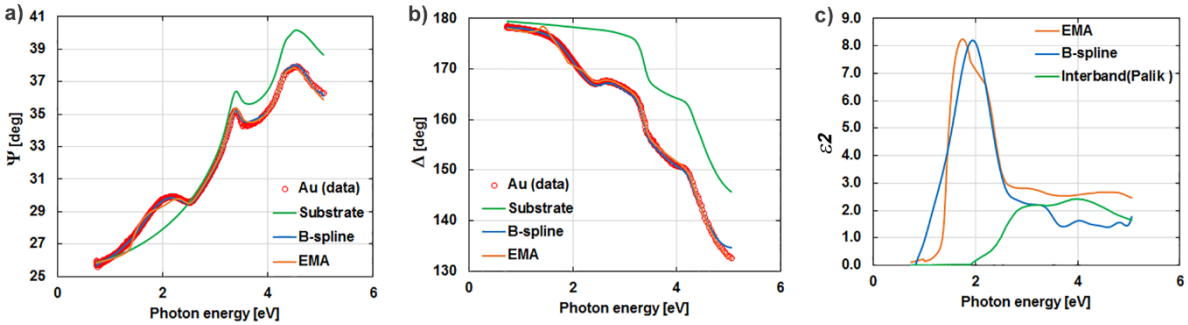

Fig. 7: Ellipsometer angles Ψ (a) and Δ (b) of a gold film of almost 3 nm nominal film thickness (QCM) and of the silicon wafer substrate. The EMA and B-spline model fit to the gold data are also shown in a) and b). Permittivity (ε2 only) as calculated from the model fits to the data together with the interband region of Palik's optical data are plotted in (c).

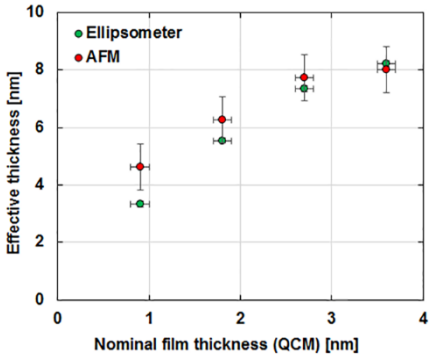

Fig. 8: Ellipsometer and AFM determined effective film thickness of gold deposits plotted versus the in-situ determined amount or nominal layer thickness with QCM.

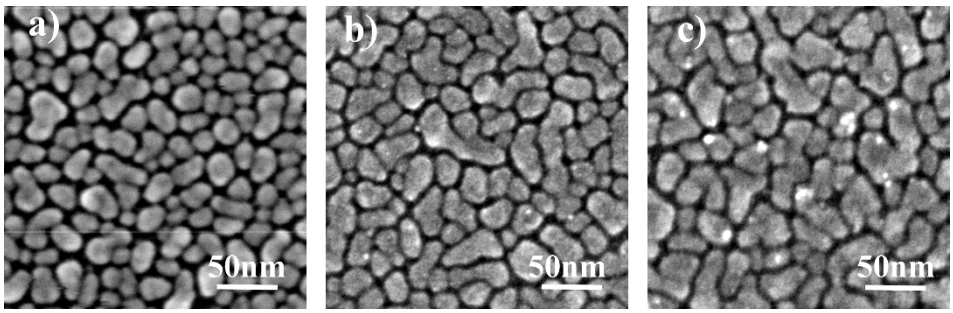

Fig. 9: 250 nm x 250 nm SEM images of 4.5 nm nominal thickness copper films with different growth rates: with a) a rate of 0.006 nm/s, b) a rate of 0.02 nm/s and c) a rate of 0.08 nm/s.

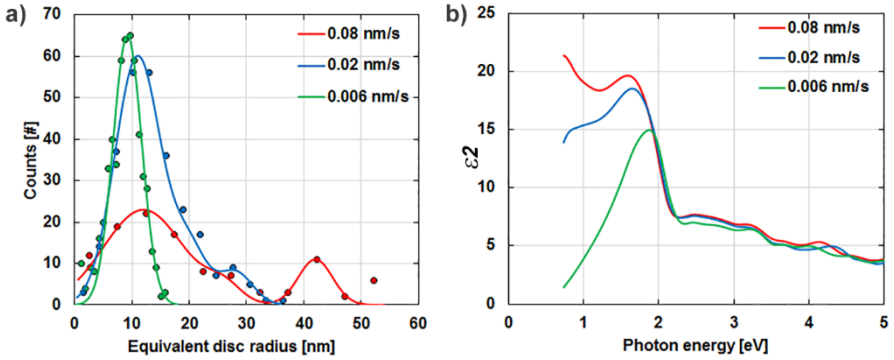

Fig. 10: Statistics on copper nano-cluster footprint from SEM images of 4.5 nm nominal thickness copper films with different growth rates in a). In b) corresponding permittivity as determined from in-situ ellipsometer data. The labels indicate the used growth rate.

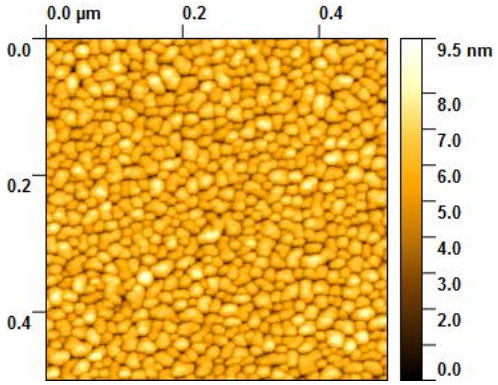

Fig. 11: 500 nm x 500 nm AFM image of a 4.5 nm nominal thickness copper film grown at 0.006 nm/s.

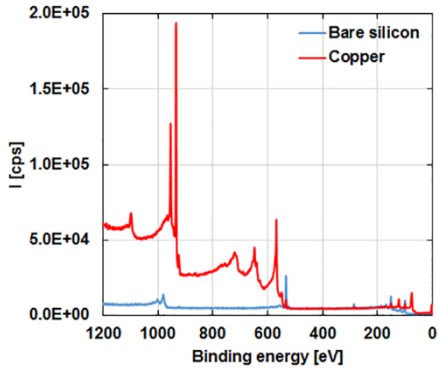

Fig. 12: In vacuum XPS survey of the silicon substrate before and after 4.5 nm copper deposition.

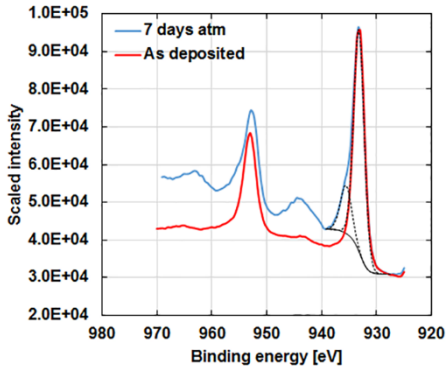

Fig. 13: XPS of the Cu2p peak of 4.5 nm copper as deposited in vacuum and after 7 days exposed to atmospheric conditions. The dashed curves are a fit to the $Cu2p_{3/2}$ part of the sample after 7 days in atmospheric conditions.

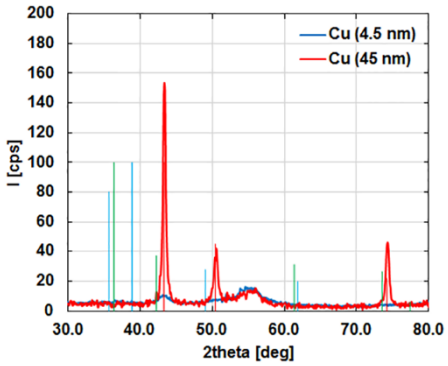

Fig. 14: Fixed angel XRD of 45 nm thick and 4.5 nm thin copper. The bars indicate library positions and relative intensities for copper in a metallic state (red), in a Cu^{1+} state of Cu_2O (green) and in a Cu^{2+} state of CuO (blue).

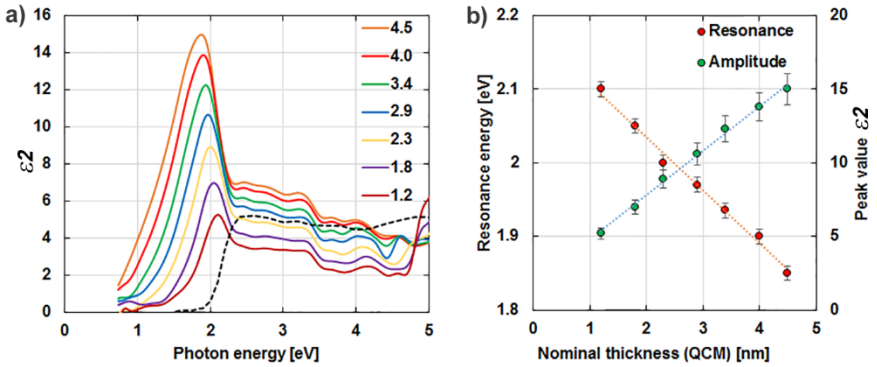

Fig. 15: Permittivity (ε2) of metallic copper as determined from real-time ellipsometer data (a) and in b) the plasmon resonance position and amplitude. The labels in (a) indicate the nominal film thickness (QCM) in nanometers and the dashed line is Palik's interband region.

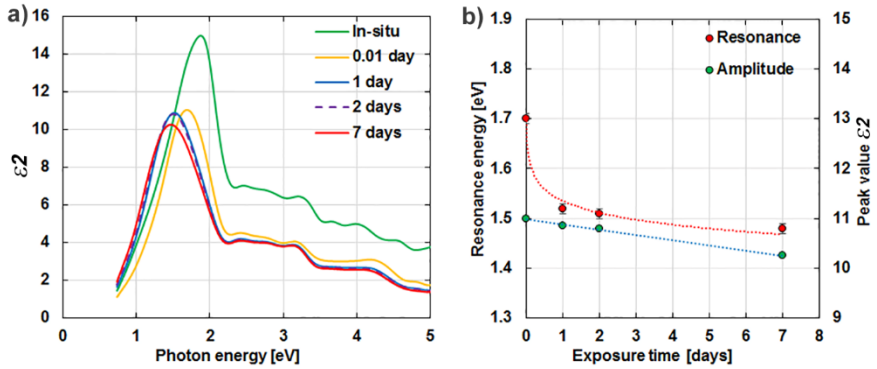

Fig. 16: Permittivity data for 4.5 nm (QCM) thick copper in-situ and ex-situ (a). The resonance positions and amplitudes of different exposure times (ex-situ) are shown in (b).